Classification of prostate cancer using a protease activity nanosensor library

Jaideep S. Dudani[a,b], Maria Ibrahim[a,c], Jesse Kirkpatrick[a,c], Andrew D. Warren[a,c,1], and Sangeeta N. Bhatia[a,c,d,e,f,g,2]

[a]Koch Institute for Integrative Cancer Research, Massachusetts Institute of Technology, Cambridge, MA 02139; [b]Department of Biological Engineering, Massachusetts Institute of Technology, Cambridge, MA 02139; [c]Harvard–MIT Division of Health Sciences and Technology, Institute for Medical Engineering and Science, Massachusetts Institute of Technology, Cambridge, MA 02139; [d]Department of Electrical Engineering and Computer Science, Massachusetts Institute of Technology, Cambridge, MA 02139; [e]Department of Medicine, Brigham and Women's Hospital, Harvard Medical School, Boston, MA 02115; [f]Broad Institute of Massachusetts Institute of Technology and Harvard, Cambridge, MA 02139; and [g]Howard Hughes Medical Institute, Cambridge, MA 02139

Edited by John A. Rogers, Northwestern University, Evanston, IL, and approved August 1, 2018 (received for review March 27, 2018)

Improved biomarkers are needed for prostate cancer, as the current gold standards have poor predictive value. Tests for circulating prostate-specific antigen (PSA) levels are susceptible to various noncancer comorbidities in the prostate and do not provide prognostic information, whereas physical biopsies are invasive, must be performed repeatedly, and only sample a fraction of the prostate. Injectable biosensors may provide a new paradigm for prostate cancer biomarkers by querying the status of the prostate via a noninvasive readout. Proteases are an important class of enzymes that play a role in every hallmark of cancer; their activities could be leveraged as biomarkers. We identified a panel of prostate cancer proteases through transcriptomic and proteomic analysis. Using this panel, we developed a nanosensor library that measures protease activity in vitro using fluorescence and in vivo using urinary readouts. In xenograft mouse models, we applied this nanosensor library to classify aggressive prostate cancer and to select predictive substrates. Last, we coformulated a subset of nanosensors with integrin-targeting ligands to increase sensitivity. These targeted nanosensors robustly classified prostate cancer aggressiveness and outperformed PSA. This activity-based nanosensor library could be useful throughout clinical management of prostate cancer, with both diagnostic and prognostic utility.

activity-based nanosensors | proteolytic enzymes | prostate cancer | diagnostic biomarkers | prognostic biomarkers

The lifetime risk for a US male to be diagnosed with prostate cancer is 1 in 6, yet mortality from this disease is only 1 in 35 (1). This discrepancy highlights the need for improved prognostication and management that could be enabled by accurate biomarkers (2). While prostate-specific antigen (PSA) is the clinical blood biomarker standard, it is susceptible to various noncancer comorbidities. For example, infection and benign prostatic hyperplasia (BPH) are the most common sources of elevated PSA (1). Factors such as the time since a benign condition and PSA half-life impact the performance of this biomarker (3, 4), which contributes to its poor predictive value: Only about 30% of men with elevated PSA have cancer detected upon biopsy (1). Further, biopsies sample only 1/1,000th of the prostate, which contributes to missing 30% of patients who bear high-grade cancer (5). Thus, a large fraction of the patients classified as low risk will progress and be at risk for recurrence. PCA3 is another biomarker that has been studied recently, but it is not as widely implemented and not recommended for use at the time of initial biopsy, according to National Comprehensive Cancer Network (NCCN) guidelines (6). Better biomarkers with lower susceptibility to benign false positives and improved ability to distinguish aggressive from indolent disease are needed.

Aberrantly expressed proteases are candidates for cancer biomarkers, as they play critical roles in almost every hallmark of cancer (7). In fact, PSA is a protease in the Kallikrein family (KLK3), and is regulated by androgen signaling. KLK2, another member in the family, may also serve as a meaningful biomarker in prostate cancer, as demonstrated recently using a radiolabeled antibody to track androgen deprivation therapy (8). This strategy of imaging active proteases in prostate cancer has been applied to several other enzymes, such as urokinase plasminogen activator (uPA), which is up-regulated in aggressive prostate cancer (9). While these strategies show promise, they each only address one aspect of prostate cancer, such as imaging the androgen receptor axis. Additionally, the reliance on imaging as a read-out requires capital-intensive equipment and precludes simultaneous measurement of multiple enzymes. The ability to integrate multiple signals has shown significant promise in cancer diagnostics, such as the ConfirmMDx for Prostate Cancer (10), OncotypeDX Prostate Cancer assay (11), and the Prolaris Prostate Cancer test (12), although these approaches require invasive biopsies. An ideal protease activity test would therefore integrate many prostate cancer-specific signals in a noninvasive platform.

We have developed injectable activity-based nanosensors (ABNs) that, in response to protease cleavage in the tumor microenvironment, release barcoded reporters detectable in the urine (13–15). We applied this concept to prostate cancer, with a focus on stratifying disease by first performing transcriptomic and proteomic analysis to identify prostate cancer-associated proteases overexpressed in cancer tissue relative to healthy tissue, as well as proteases that differentiate higher- and lower-grade cancers. Next, we screened a panel of protease substrates for activity against these disease-associated proteases and formulated a 19-plex ABN library. We evaluated this library using in vitro and in vivo models of human prostate cancer that recapitulated the protease expression

Significance

Prostate cancer is the most common noncutaneous cancer in men, but there is a need for better biomarkers that can identify aggressive disease. Here, we describe a bottom-up approach to design nanosensors to detect and classify prostate cancer. We used transcriptomic and proteomic analysis to identify proteolytic enzymes that are dysregulated in human prostate cancer and built a library of nanosensors to measure their activity in vivo using multiplexed urinary readouts. In mouse models, we demonstrated that these nanosensors could classify aggressive prostate cancer and outperform a serum biomarker. This library could be deployed as a screening test to identify patients with higher-risk prostate cancer at the time of screening.

Author contributions: J.S.D., M.I., J.K., A.D.W., and S.N.B. designed research; J.S.D., M.I., and J.K. performed research; J.S.D. and A.D.W. contributed new reagents/analytic tools; J.S.D., M.I., J.K., A.D.W., and S.N.B. analyzed data; and J.S.D. and S.N.B. wrote the paper.

Conflict of interest statement: J.S.D. and S.N.B. are listed as inventors on a patent application related to this work. A.D.W. is currently an employee of Glympse Bio. S.N.B. is a shareholder of and consultant to Glympse Bio.

This article is a PNAS Direct Submission.

[1]Present address: Glympse Bio, Cambridge, MA 02139.

[2]To whom correspondence should be addressed. Email: sbhatia@mit.edu.

This article contains supporting information online at www.pnas.org/lookup/suppl/doi:10.1073/pnas.1805337115/-/DCSupplemental.

patterns seen in human cancers. Finally, we modified nanosensors with integrin-targeting peptides to enhance sensitivity and achieved robust classification of aggressive cancer and outperformed PSA for detection.

Results

Human Transcriptome Analysis Identifies Candidate Protease Biomarkers. We set out to systematically identify proteases expressed in human prostate cancer, formulate and build ABNs to measure their activity, and test the ABNs (Fig. 1*A*). The ABN platform comprises three components: a nanoparticle core that determines biodistribution and prevents urine accumulation of unliberated reporters, peptide substrates that are cleaved by target endoproteases, and urinary reporter barcodes paired to each substrate.

We queried transcriptomic data in The Cancer Genome Atlas (TCGA) to identify proteases overexpressed in prostate cancer samples versus normal adjacent tissue (NAT) samples (Fig. 1*B*). Out of over 150 secreted and membrane-bound endoproteases in this dataset, 26 were expressed in tumors at levels at least 1.5-fold over NAT (panel termed "PRAD" to represent proteases overexpressed in prostate adenocarcinoma). Next, we analyzed the same TCGA dataset to identify proteases that differentiated Gleason 7 to 10 samples from lower-grade Gleason 6 samples (Fig. 1*C*) because Gleason 6 lesions have been shown to lack many of the hallmarks of cancer (5). A list of 17 protease genes was elevated in the higher-scoring Gleason samples (panel termed "AGGR" to represent proteases overexpressed in aggressive cancer) (Fig. 1*C*). Nine proteases were present on both lists (*SI Appendix*, Fig. S1*A*). A subset of proteases from these analyses offered good classification potential, based on area under the receiver operating characteristic (AUROC) curve analysis, for distinguishing cancer from normal (max AUROC = 0.93) and aggressive from indolent (max AUROC = 0.73; *SI Appendix*, Fig. S1 *B* and *C*). These proteases were predominantly metalloproteinases (MPs) and serine proteases (SPs). Notably, we queried the same TCGA samples to look for concomitant protease inhibitor up-regulation and observed that many tissue inhibitors of MPs and serine protease inhibitors were expressed at reduced levels in cancer samples (*SI Appendix*, Fig. S1*D*), highlighting broad proteolytic dysregulation. We filtered the protease lists based on several practical criteria, including availability of recombinant protease for use in substrate development, organ expression patterns using the Genotype-Tissue Expression (GTEx) portal, and knowledge of substrate specificities, resulting in a list of 14 candidate proteases (*SI Appendix*, Fig. S1*A*).

Importantly, while patients with high expression of proteases identified from the cancer vs. normal (PRAD) analysis did not have poorer disease-free survival as quantified by Kaplan–Meier analysis (Fig. 1*D*), patients with high expression of proteases in the AGGR list exhibited significantly poorer disease-free survival (Fig. 1*E*). This analysis underscores the importance of selecting biomarkers with good prognostic performance, rather than focusing solely on diagnosis. In an independent dataset (16), high expression of proteases in AGGR corroborated the same significantly poorer disease-free survival (*SI Appendix*, Fig. S2), further validating these biomarkers.

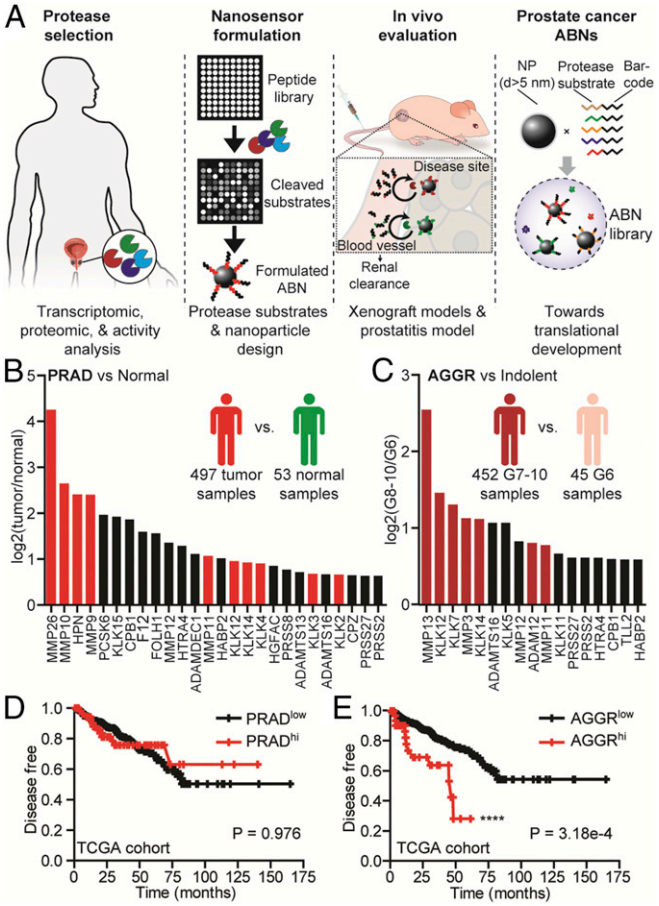

Fig. 1. In silico identification of candidate proteases for an ABN library. (*A*) Project workflow. Protease targets were identified, substrates were designed and tested, and ABNs were generated to evaluate in vivo and for further translational development. (*B*) Analysis of overexpressed proteases in prostate cancer samples (PRAD) vs. NAT (Normal) or (*C*) in Gleason 7 to 10 samples (AGGR) vs. Gleason 6 samples (Indolent). Hits from each analysis are shown in red. (*D* and *E*) Disease-free survival stratification in the TCGA cohort based on expression of proteases in the (*D*) PRAD list and (*E*) AGGR list. (*D* and *E*: log-rank *T* test.)

Experimental Validation of Increased Protease Abundance and Activity in Human Prostate Cancer. To confirm that the transcriptome-based candidates were expressed, we applied a high throughput proteomics assay (SOMAscan) (17). Five prostate tumor samples (Gleason sums from 6 to 9) and five matched NAT samples were analyzed for protein abundance (*SI Appendix*, Fig. S3), and the results were compared with the two sets of transcriptomic hits (Fig. 2 *A* and *B*); we also screened for any candidates that were not identified at the transcript level (Fig. 2*C*). In the case of the PRAD list, all hits but one (KLK3, or PSA) were elevated in tumor samples compared with their average abundance in NAT, but no clear trends were observed in samples with higher Gleason scores (Fig. 2*A*). The lack of PSA protein elevation in the tumor samples highlights its poor performance as a biomarker to distinguish cancer from other conditions. In contrast, larger effect sizes were observed for the protein abundance of each of the proteases listed in the AGGR set, except for KLK7; these results mirrored the transcriptomic data, with clear differences in effect size observed in higher Gleason score tumors (Fig. 2*B*). Finally, the SOMAscan data identified two additional proteases (uPA and PRSS3) that were more abundant in the tumor samples (Fig. 2*C*), and are well annotated in the literature as playing a role in aggressive prostate cancer (9, 18). The modest effect sizes observed could be explained by the comparison with NAT samples, which includes reactive stroma, as well as the low tumor content in several samples (*SI Appendix*, Fig. S3). In this vein, a recent analysis of TCGA NAT samples relative to normal tissue (GTEx) demonstrated that NAT samples do not fully reflect normal tissue gene expression (19).

To examine protein expression of candidate proteases in a tissue architecture-dependent method and compare abundance in inflamed tissue, we selected one protease from each list and type (MP and SP) and performed immunohistochemical (IHC) staining on human prostate cancer tumor microarrays (TMAs). MMP26 and KLK14 stained positively in tumor samples, with a higher intensity of staining for KLK14 (Fig. 2*D* and *SI Appendix*, Fig. S4). Notably, both proteases were expressed at elevated levels

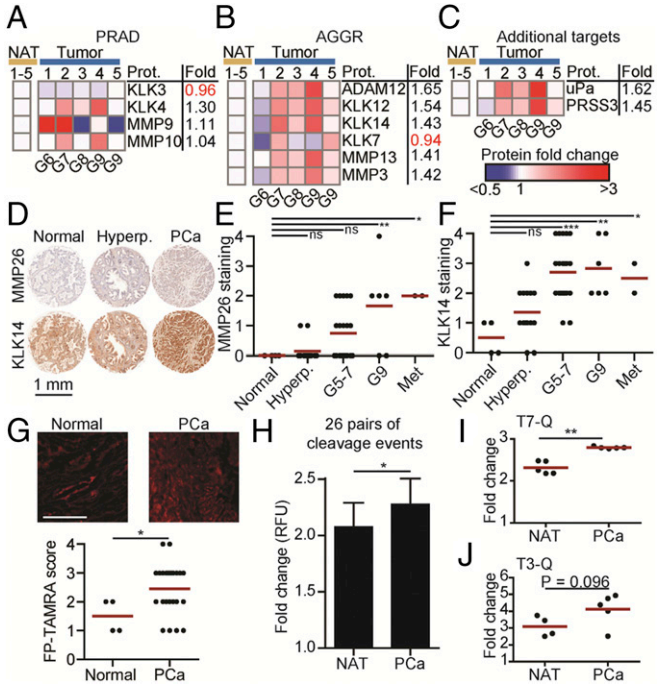

Fig. 2. Experimental validation of increased protease abundance and activity in PCa. (*A*–*C*) SOMAscan assay results from five tumor and paired NAT samples comparing protein abundance of (*A*) PRAD list hits, (*B*) AGGR list, and (*C*) additional targets. (*D*) Representative images from IHC staining of proteases in a prostate cancer TMA. Hyperp., hyperplasia, inflammation, benign samples. (*E* and *F*) TMA staining score of both proteases. (*G*) Serine hydrolase ABP labeling (red) in a human prostate cancer TMA. (Scale bar: 500 μm.) (*H*) Human cancer samples and NAT samples were tested against FRET peptide substrates. Data shown represent combined samples and substrates with paired cleavage data. (*I* and *J*) FRET cleavage results from two metalloproteinase substrates in multiple tumor samples compared with NAT. (*E* and *F*, one-way ANOVA with Tukey's multiple comparison test; *G*, unpaired *t* test; *H*, Wilcoxon matched-pairs test; *I* and *J*, paired *t* test; $*P < 0.05$, $**P < 0.01$, $***P < 0.001$.)

in tumors compared with normal, and with inflamed or hyperplastic samples (*SI Appendix*, Fig. S4); further, these proteases stained positive in sections from metastases (Fig. 2 *E* and *F*).

Next, we sought to assay enzyme activity in prostate cancer samples. Activity-based probes (ABPs) that specifically bind to active hydrolases have been used to detect protease activity in human samples (20). Thus, we applied a serine hydrolase probe, fluorophosphonate-TAMRA (FP-TAMRA; TAMRA is a fluorophore) to fresh-frozen samples, which maintain proteolytic activity (15, 20), and labeled tumor cells in sections of a xenograft tumor derived from a human prostate cancer cell line, 22Rv1 (*SI Appendix*, Fig. S5*A*). This labeling was mitigated by the addition of a small molecule serine protease inhibitor called AEBSF. When applied to a fresh-frozen human prostate cancer TMA, FP-TAMRA labeled prostate cancer samples more than normal control samples (Fig. 2*G* and *SI Appendix*, Fig. S5*B*).

As MP ABPs are less robust than serine ABPs, we used a FRET peptide substrate-cleavage assay to assay for MMP activity in the same tissue set we evaluated by SOMAscan. Given the minimal tissue material available, each sample was evaluated with only a subset of substrates in duplicate (*SI Appendix*, Fig. S6*A*). Multiple substrates were cleaved to a greater extent in tumor samples (*SI Appendix*, Fig. S6*B*). Consistent with protein increases detected by SOMAscan, the cleavage signal elevation was modest, yet, in analyzing the 26 sets of paired measurements, significantly higher cleavage was detected in tumor samples (Fig. 2*H*). In the case of two MMP-sensing substrates, T7 and T3 (13), signal was elevated across the majority of tumor samples, indicating a pattern of increased MMP activity in prostate cancer (Fig. 2 *I* and *J*).

Given our goal to establish an ABN library to both diagnose and classify prostate cancer, we integrated our analyses thus far and finalized a list of 15 proteases upon which to build our nanosensor library (*SI Appendix*, Table S1).

Development of Nanosensor Library Responsive to Selected Metalloproteinases and Serine Proteases. With an identified set of MPs and SPs, we developed a panel of substrates to measure their activity. We screened a panel of 58 FRET-paired peptide substrates (labeled T1-58-Q, where Q denotes quenched; *SI Appendix*, Table S2) for cleavage by the 15 selected proteases. To account for background cleavage in circulation, we included Thrombin, Factor Xa, and human plasma as negative filters (*SI Appendix*, Fig. S7*A*). The library comprised peptides with diverse physiochemical properties to provide broad coverage (*SI Appendix*, Fig. S7*B*), and kinetic parameters of cleavage of the FRET-paired substrates by recombinant proteases were measured and *z*-score normalized by protease (Fig. 3*A* and *SI Appendix*, Fig. S7 *C* and *D*). Substrates were grouped by hierarchical clustering to remove substrates with overlapping cleavage patterns, as they would not provide any orthogonal insight, resulting in a down-selected panel of 26 substrates.

As these substrates will be used in vivo, conjugation to a nanoparticle with robust accumulation in the prostate was needed. Thus, we performed a biodistribution study with three fluorophore-labeled carrier candidates and tested for their biodistribution following i.v. injection. Relative to two iron oxide carriers, a multivalent PEG polymer (*SI Appendix*, Fig. S8*A*) accumulated more in the prostate (Fig. 3*B*), and less in spleen and liver (*SI Appendix*, Fig. S7 *B* and *C*). Thus, we conjugated our peptide substrates to a PEG core and tested their cleavage profile (Fig. 3*C*). While most substrates were cleaved similarly with and without PEG coupling, some discrepancies were observed, suggesting the

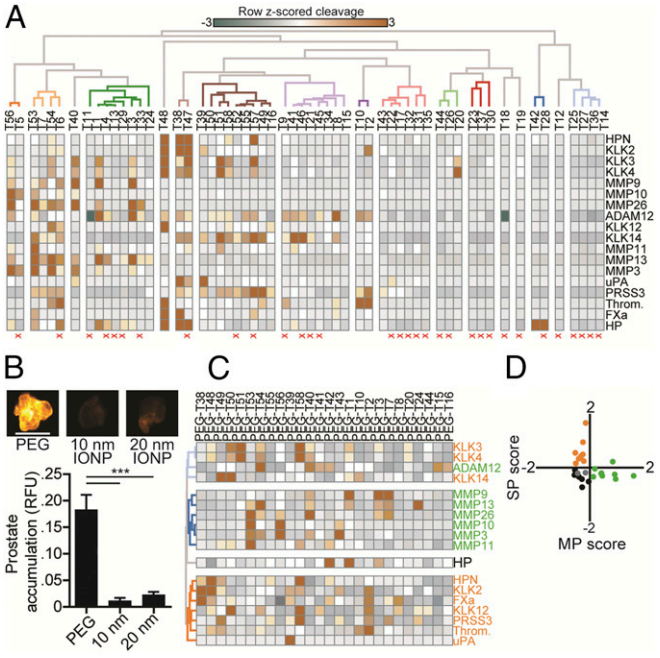

Fig. 3. Development of ABN library responsive to selected metalloproteinases and serine proteases. (*A*) Hierarchical clustering was used to identify similarly cleaved substrates, which were subsequently eliminated for a second screen (red x). (*B*) Different nanoparticle formulations were injected i.v. and detected by fluorescent scan of prostate 6 h after treatment. (Scale bar: 1 cm.) One-way ANOVA with Tukey's multiple comparison test; $***P < 0.001$. (*C*) Selected substrates were coupled to PEG and exposed to recombinant proteases, and cleavage data across the 26 PEG-peptide conjugates were *z*-scored and clustered, as above. (*D*) Each substrate was assigned an MP and SP score based on mean cleavage of each substrate across proteases in the family.

need for empirical evaluation of peptide cleavage in any given formulation (*SI Appendix*, Fig. S9). Further mechanistic understanding of this variability may improve the development of ABN technology by identifying optimal surface presentation. Notably, analysis of the substrate cleavage profiles largely grouped MPs separately from SPs (Fig. 3*C*). Furthermore, MP and SP cleavage scores were calculated for each peptide and revealed an orthogonal pattern to their cleavage specificity: Peptides that were well cleaved by MPs were poorly cleaved by SPs (Fig. 3*D*). Some substrates were cleaved specifically by a single protease on our biomarker list, whereas others were cleaved by multiple or all members of the enzyme family tested (*SI Appendix*, Table S3). Ultimately, we removed all but two substrates that were poorly cleaved by both enzyme families from the final panel to yield a 19-plex ABN library that offers broad coverage of relevant prostate cancer-expressed proteases, and thus should enable predictive signature building.

Evaluation of ABN Library Against Cancer Cell Lines in Vitro and in Vivo. We first evaluated the prostate cancer ABN library in vitro using human cell lines. To select representative models, we used protease gene expression across seven cancer cell lines from the Cancer Cell Line Encyclopedia (CCLE) (Fig. 4*A*). Hierarchical clustering of these data grouped the cell lines based on androgen receptor status, validating our hypothesis that protease expression correlates with clinically meaningful prostate cancer status (Fig. 4*A*). We noted that the PC3 cell line differentially expressed many of the proteases included in the AGGR list that discerns tumors by Gleason stage (*SI Appendix*, Table S1). Further, the PC3 line is undifferentiated, AR−, PSA−, has metastatic potential, and is derived from a bone metastasis (21). In contrast, the 22Rv1 cell line is poorly differentiated, AR+, PSA+, lacks metastatic potential, and is derived from serial passaging of a primary tumor. We performed a transwell matrigel invasion assay and observed that PC3 exhibits greater invasion capacity than 22Rv1, and was significantly inhibited by broad-spectrum protease inhibitors, suggesting this invasion was proteolytically driven (Fig. 4*B*).

Given their distinct protease profiles, we selected the 22Rv1 and PC3 lines to test the activity of the ABN library, and quantified cleavage of the 19-plex fluorogenic ABNs in supernatant. Consistent with the library design, overall cleavage activity for both lines was reduced in the presence of marimastat (MMP inhibitor) or AEBSF (serine protease inhibitor), but not E64 (cysteine protease inhibitor) (Fig. 4*C* and *SI Appendix*, Fig. S10). Additionally, there were cell line-specific cleavage patterns, with greater overall cleavage observed in the PC3 cells (*SI Appendix*, Fig. S8 *A* and *B*).

To evaluate whether the panel of protease-responsive substrates can detect and classify disease in vivo, we formulated substrates with urinary reporters to generate in vivo ABNs. Based on our previous work (22, 23), we initially barcoded one ABN sensor using a stable biotinylated D-stereoisomer of glutamate fibrinopeptide for detection (*SI Appendix*, Fig. S11*A* and Table S2). These short peptides have previously been shown to reliably accumulate in the urine following proteolytic liberation from the carrier nanoparticle. We optimized the time point of urine collection by tracking urine signal generation in healthy mice and identified the optimal collection window to be between 0 min and 60 min postinjection (*SI Appendix*, Fig. S11*B*). Additionally, we observed no difference in signal when a second injection was administered to healthy mice 2 wk later (*SI Appendix*, Fig. S11*C*).

In mice bearing tumor xenografts derived from 22Rv1 cells, the ABNs accumulated in the tumors (*SI Appendix*, Fig. S11*D*). We detected an increased urinary signal from reporters liberated by proteolysis of the T7 substrate in 22Rv1 xenograft-bearing mice (Fig. 4*D*), and the performance of the sensor was equivalent when coupled to an alternately barcoded reporter (*SI Appendix*, Fig. S11*E*). To confirm the signal increase was due to proteolysis in the tumor, we tested the protease activity of tumor homogenates ex vivo and observed that T7 sensor cleavage was diminished in the presence of MMP inhibitor marimastat (Fig. 4*E*). We also performed an in vivo protease activity imaging study using a red-shifted FRET paired T7 substrate, which showed greater fluorescence signal in the tumor compared with the liver (*SI Appendix*, Fig. S11*F* and Table S2).

Having achieved this proof-of-concept urine monitoring of protease activity with a single substrate, we tested the entire ABN library in vivo with an emphasis on identifying reporters to differentiate mice bearing more aggressive (PC3) versus less aggressive (22Rv1) xenografts. To quantify cleavage of the entire library in urine, we barcoded the substrates using a next generation of mass-encoded reporters built upon our previous isobar coded reporters method (*SI Appendix*, Fig. S12*A*) (13). This reengineered sensor library enables increased multiplexing by uniquely labeling each peptide with stable ^{13}C and ^{15}N atoms, allowing for quantitation of reporter barcodes across a large dynamic range using liquid chromatography–tandem mass spectrometry (*SI Appendix*, Fig. S12 and Table S4).

To account for variability in glomerular filtration rate, urine volume, and hydration state, we coinjected a free reporter (not coupled to PEG). We serially administered the 19-plex ABN library i.v. to PC3 tumor-bearing mice over the course of tumor development. As tumors increased in size, we observed an increase in the aggregate urine signal, expressed as the sum of all disease-sensitive reporters normalized to the coadministered free reporter (Fig. 4*F*).

Next, we sought to determine the ability of the 19-plex library to classify PC3 from 22Rv1 tumor-bearing mice. Using the

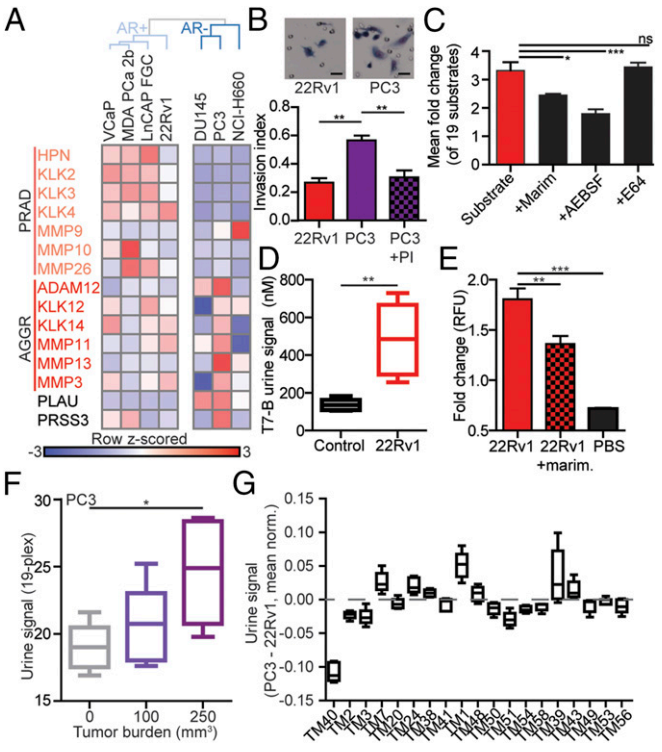

Fig. 4. Evaluation of prostate 19-plex ABN library in vitro and in vivo. (*A*) Protease expression across prostate cancer cell lines from CCLE. (*B*) Matrigel invasion assay performed with PC3 and 22Rv1 cells. PI, protease Inhibitor mixture. (Scale bar: 20 μm.) (*C*) The 22Rv1 supernatant was incubated with the fluorogenic ABN library, and fluorescence increase was measured with or without marimastat (marim), AEBSF, or E64 inhibitors. (*D*) Urine signal detected 1-h postinjection of PEG-T7-B in mice with or without 22Rv1 xenografts. (*E*) Ex vivo cleavage signal of the T7 reporter by 22Rv1 tumor homogenates. (*F*) Aggregate urine signal after injection of the full 19-plex library with mass-encoded barcodes in mice bearing PC3-derived xenografts. (*G*) Mean normalized reporter signal changes from healthy mice were calculated, and the difference between PC3 and 22Rv1 is plotted for each reporter. (*B*, *C*, *E*, and *F*, one-way ANOVA with Tukey's multiple comparison test; *D*, student's *t* test; $*P < 0.05$, $**P < 0.01$, $***P < 0.001$.)

mass-encoded reporters to examine the cleavage of each individual sensor, we focused on an early time point and observed that several substrates were differentially cleaved between animals bearing similarly sized xenografts (~100 mm^3) from the more (PC3) versus less aggressive (22Rv1) cell lines (Fig. 4*G* and *SI Appendix*, Fig. S13). Overall, the cleavage profile differences between the two cohorts agree with each cell line's protease expression patterns (Fig. 4*A*) and the substrate specificity of each protease (Fig. 3*C*). For example, substrates T24 and T39 show higher relative urine signal change in mice bearing PC3 xenografts compared with 22Rv1 xenografts; in vitro, these substrates are cleaved by proteases overexpressed in PC3 cells, MMP13 and uPA. Other substrate sensors that are predominantly cleaved by proteases expressed by 22Rv1 cells show preferential signal generation in 22Rv1-bearing mice; for example, T40 and T51 are cleaved by MMP26 and KLK4, respectively.

An Integrin-Targeted ABN Library Subset Robustly Classifies Aggressive Prostate Cancer. One advantage of a highly multiplexed library is the capacity to nominate a smaller subset of sensors for a specific application. We integrated the results of testing the 19-plex library in vitro (fluorogenic) and in vivo (mass-encoded) against PC3 and 22Rv1 cells to select a minimal subset of ABNs for a more practical diagnostic platform with simpler urinary readouts (23).

As stated above, urinary reporters released from T24 and T39 sensors, which are selectively cleaved by MMP13 and uPA (*SI Appendix*, Fig. S14*A*), were elevated in PC3-bearing mice compared with 22Rv1 mice and were also cleaved differentially by PC3 cell supernatants in vitro (*SI Appendix*, Fig. S10). Consistent with this result, PC3 flank xenografts expressed MMP13 and uPA more than 22Rv1 flank xenografts (Fig. 5*A*). Interestingly, both of these proteases play a role in bone metastasis, which is the source of the PC3 cell line (24), and also a common site of metastasis for prostate cancer. We also nominated T7 for our targeted ABN panel, as it gave rise to urine signals in both 22Rv1 and PC3 mice and was used in our earlier optimization experiments.

Noting that the effect sizes we observed were small, consistent with the untargeted nature of our nanosensors, we sought to increase the performance of our selected subset of sensors by using tumor-targeting peptides. We have previously shown that adding integrin-targeting, tumor-penetrating peptides can increase performance of ABNs (15). A cyclic form of RGD, iRGD, enables greater tumor penetration and delivery by binding $\alpha_v\beta_3$/β_5 integrins (25). After confirming that α_v integrins were overexpressed in human prostate cancer (26) by staining a TMA (Fig. 5*B* and *SI Appendix*, Fig. S14*B*), and that both PC3 and 22Rv1 xenografts stained for high levels of αv integrins (Fig. 5*C*), we modified our ABN design to incorporate iRGD. We initially tested whether coupling iRGD to the ABN increased performance of T7 nanosensors in mice bearing 22Rv1-derived xenografts at 100-mm^3 aggregate tumor burden. Signal derived from iRGD-modified T7 ABNs was significantly greater than that produced by unmodified ABNs (Fig. 5*D*).

Guided by this positive test, we next produced a three-plex of iRGD-modified ABNs (iRGD-ABNs) using substrates T7, T24, and T39 (*SI Appendix*, Table S2). To simplify urinalysis, these ABNs were designed to release biotinylated urinary reporters to enable ELISA-based readouts. Following i.v. injection of the three-plex iRGD-ABNs, the combined urine reporter signal was elevated in both 22Rv1-bearing and PC3-bearing animals compared with controls (Fig. 5 *E*, *Left* and *F*, *Left*). Notably, this urine diagnostic sensor increase was both significant and more robust than serum PSA elevation in both cohorts (Fig. 5 *E*, *Right* and *F*, *Right*). The pattern is more striking in PC3-bearing mice as this tumor is PSA negative (*SI Appendix*, Fig. S14 *C* and *D*), suggesting the combination of signal amplification from protease activity and concentration into urine concentration could be more predictive than serum biomarkers (15). Additionally, PSA measurements in mice may overestimate its sensitivity, as there is no mouse homolog of PSA (27).

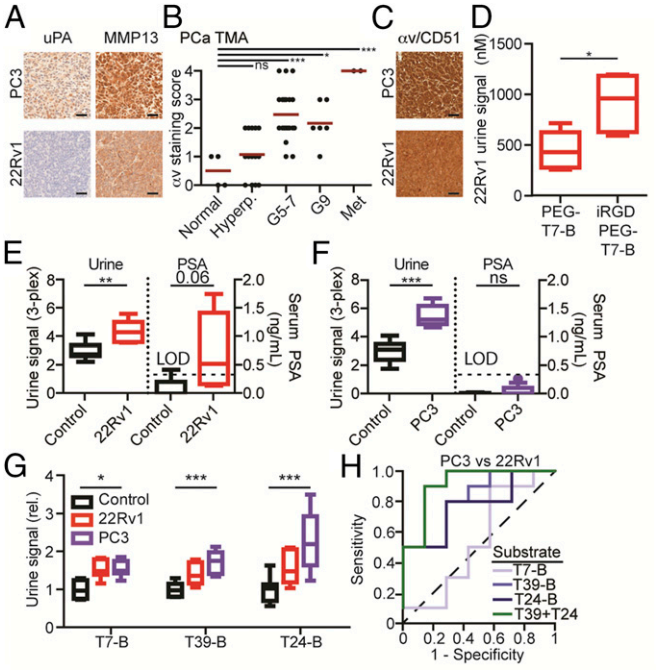

Fig. 5. Integrin-targeting of a subset of ABN library for increased sensitivity. (*A*) IHC staining for uPA and MMP13 in PC3 and 22RV1 tumor xenograft sections. (*B*) The α_v integrin staining of a prostate cancer TMA. (*C*) Positive staining of α_v in both 22Rv1 and PC3 sections. (Scale bar for *A* and *C*: 50 μm.) (*D*) Urine signal in 22Rv1-bearing mice after injection of iRGD-modified or unmodified PEG-T7 ABN. (*E* and *F*) Combined urine signal from multiplexed iRGD ABNs (T7, T39, and T24) was evaluated in (*E*) 22Rv1 and (*F*) PC3 xenografted mice (left half of each graph), in parallel with serum PSA testing in the same animals (right half of each graph). (*G*) Urine signal from the mice shown in *E* and *F* presented for each of the three-plex substrates. (*H*) ROC curve analysis demonstrates robust predictive ability of T39 (AUROC = 0.814) and T24 (AUROC = 0.771), which is enhanced when the two substrate signals are combined (AUROC = 0.914, green). T7 provides poor classification (AUROC = 0.543) between the two groups. Dashed line represents an AUROC of 0.5, and a perfect AUROC is 1.0. (*D*, student's *t* test; *E* and *F*, one-way ANOVA with Tukey's multiple comparison test; *G*, two-way ANOVA with Tukey's multiple comparison test; $*P < 0.05$, $**P < 0.01$, $***P < 0.001$.)

We next tested whether the three-plex iRGD-ABNs could classify distinct prostate cancer tumors. When the individual reporter readouts were compared, mice bearing PC3 tumors gave rise to significantly greater cleavage of both the uPA (T39) and MMP13 (T24) substrates relative to 22Rv1 (Fig. 5*G*), consistent with the relative protease expression profile of the cell lines. Both sets of tumor-bearing mice generated T7 urine signals that were elevated relative to control animals, but this sensor readout did not classify between the two cohorts. Based on ROC curve analysis, the T39 and T24 ABNs classified the mice bearing the more aggressive PC3-derived tumors as distinct from 22Rv1-bearing mice (Fig. 5*H*). Importantly, the sum of the uPA and MMP13 substrate signals significantly increased the classification power of the nanosensors.

Finally, a common complication of existing prostate cancer biomarkers is the high rate of false positives due to comorbidities, such as BPH and prostatitis (1). We sought to assess whether our three-plex ABNs were similarly susceptible to comorbidities by evaluating them in nonobese diabetic mice that develop prostatitis and also display prostatic hypertrophy as they age (28, 29). At 20 wk of age, prostatic hyperplasia and immune cell infiltration were noted in the prostate (*SI Appendix*, Fig. S15 *A* and *B*), but urine signal was not elevated in the older mice (*SI Appendix*, Fig. S15*C*), highlighting that these diagnostic tools are both sensitive and specific. This model represents an initial step toward defining the specificity of ABNs in animal models. This

approach needs to be systemically evaluated in humans, but several reports are encouraging, such as evidence of increased uPA activity in cancer tissue versus BPH (30) and elevated plasma levels of MMP13 and MMP9 in patients with cancer versus BPH (31).

Discussion

We applied a bottom-up approach to design, build, and test a panel of ABNs to detect and classify prostate cancer. First, we used transcriptomic and proteomic tools to nominate proteases that identify and stratify prostate cancer in human samples. Next, we designed substrates to detect these proteases and built an ABN library using these substrates. The resulting 19-plex ABN library was evaluated in vitro and in vivo using mass-encoded barcodes for urinary analysis in cell line xenograft models. We identified a pair of proteases that were differentially expressed in the PC3 cell line. To increase performance, we modified a panel of ABNs with iRGD to bind overexpressed integrins in prostate cancer. The iRGD-modified ABNs robustly classified invasive (PC3) from less invasive (22Rv1) tumor-bearing mice, and outperformed PSA as a diagnostic biomarker in these models. These ABNs did not produce false-positive results in a prostatitis mouse model. Furthermore, our prior studies that were focused on enhancing sensitivity demonstrated the ability to detect sub-5-mm ovarian cancer lesions using integrin-targeted ABNs (15).

While this diagnostic demonstration was restricted to flank xenograft cell line models, our 19-plex library of sensors can be applied to additional, representative models of prostate cancer, such as orthotopic tumors and the Hi-Myc mouse (32). Additionally, it would be interesting to evaluate this library of ABNs as a pharmacodynamic biomarker for androgen deprivation therapies. Further reduction to the risk of false positive signals could be achieved by more in-depth benchmarking of net protease activity against BPH and other comorbidities. For example, a more systematic evaluation of the degradome (proteases and inhibitors) of a range of tissue sources and contexts using a systems biology approach could be informative, and build upon our existing analysis to improve the specificity of the selected proteases used for prostate cancer detection.

Further refinement of peptide substrates and nanoparticle formulation and dosing, such as to achieve s.c. (22) or oral delivery (33, 34), could also enhance the library's performance and enable its practical application in prostate cancer patients to improve management and outcomes. Finally, additional work needs to be completed before clinical translation, including the study of sensor specificity in the context of additional animal models of comorbidities and in human samples, as well as testing for potential immunogenicity of ABNs. This work highlights the potential ability to query biological and clinical states with ABNs.

Methods

Transcriptomic, SOMAscan, and Activity Analysis. Differential expression analysis was performed on TCGA data using SAMseq. Survival analysis was performed using cBioPortal. SOMAscan was performed at the Beth Israel Deaconess Medical Center (BIDMC) Genomics Proteomics Core. Fresh frozen prostate cancer tissue microarray was obtained from US BioChain (T6235201) and stained with FP-TAMRA (88318; Sigma) at 1 μM in PBS.

Animal Models. All animal studies were approved by Massachusetts Institute of Technology's Committee on Animal Care (CAC) (Protocol 0417-025-20). Four- to six-week-old male NCr nude mice (Taconic) were injected bilaterally with 3.5×10^6 PCa cells per flank in a 1:1 ratio of complete media and Matrigel (354234; Corning). Baseline urine measurement was obtained before xenograft implantation. Histology sectioning and staining was performed at KI Histology Core.

ACKNOWLEDGMENTS. We thank H. Fleming for critical editing of the manuscript; the KI Swanson Biotechnology Core and the High Throughput Screening Core, T. Libermann and S. Dillon at BIDMC for assistance with SOMAscan; and R. McMullin, D. Ricci, M. Gormley, and B. Radinsky (Janssen) for helpful guidance and discussion. This study was supported by Janssen Research & Development and in part by a Koch Institute Support Grant P30-CA14051 from the National Cancer Institute (Swanson Biotechnology Center), a Core Center Grant P30-ES002109 from the National Institute of Environmental Health Sciences, the Ludwig Fund for Cancer Research, and the Koch Institute Marble Center for Cancer Nanomedicine. We acknowledge support from the Ludwig Center fellowship (to J.S.D., J.K., and A.D.W.) and the National Science Foundation Graduate Research Fellowships Program (to J.S.D. and A.D.W.). S.N.B. is an HHMI Investigator.

1. Prensner JR, Rubin MA, Wei JT, Chinnaiyan AM (2012) Beyond PSA: The next generation of prostate cancer biomarkers. *Sci Transl Med* 4:127rv3.
2. Sawyers CL (2008) The cancer biomarker problem. *Nature* 452:548–552.
3. Stamey TA, et al. (1987) Prostate-specific antigen as a serum marker for adenocarcinoma of the prostate. *N Engl J Med* 317:909–916.
4. Nadler RB, Humphrey PA, Smith DS, Catalona WJ, Ratliff TL (1995) Effect of inflammation and benign prostatic hyperplasia on elevated serum prostate specific antigen levels. *J Urol* 154:407–413.
5. Klotz L, Emberton M (2014) Management of low risk prostate cancer-active surveillance and focal therapy. *Nat Rev Clin Oncol* 11:324–334.
6. Wei JT, et al. (2014) Can urinary PCA3 supplement PSA in the early detection of prostate cancer? *J Clin Oncol* 32:4066–4072.
7. Dudani JS, Warren AD, Bhatia SN (2018) Harnessing protease activity to improve cancer care. *Annu Rev Cancer Biol* 2:353–376.
8. Thorek DLJ, et al. (2016) Internalization of secreted antigen–targeted antibodies by the neonatal Fc receptor for precision imaging of the androgen receptor axis. *Sci Transl Med* 8:367ra167.
9. LeBeau AM, et al. (2015) Imaging active urokinase plasminogen activator in prostate cancer. *Cancer Res* 75:1225–1235.
10. Partin AW, et al. (2014) Clinical validation of an epigenetic assay to predict negative histopathological results in repeat prostate biopsies. *J Urol* 192:1081–1087.
11. Eeden SKVD, et al. (2017) A biopsy-based 17-gene genomic prostate score as a predictor of metastases and prostate cancer death in surgically treated men with clinically localized disease. *Eur Urol* 73:129–138.
12. Cuzick J, et al.; Transatlantic Prostate Group (2011) Prognostic value of an RNA expression signature derived from cell cycle proliferation genes in patients with prostate cancer: A retrospective study. *Lancet Oncol* 12:245–255.
13. Kwong GA, et al. (2013) Mass-encoded synthetic biomarkers for multiplexed urinary monitoring of disease. *Nat Biotechnol* 31:63–70.
14. Kwong GA, et al. (2015) Mathematical framework for activity-based cancer biomarkers. *Proc Natl Acad Sci USA* 112:12627–12632.
15. Kwon EJ, Dudani JS, Bhatia SN (2017) Ultrasensitive tumour-penetrating nanosensors of protease activity. *Nat Biomed Eng* 1:0054.
16. Taylor BS, et al. (2010) Integrative genomic profiling of human prostate cancer. *Cancer Cell* 18:11–22.
17. Mehan MR, et al. (2012) Protein signature of lung cancer tissues. *PLoS One* 7:e35157.
18. Hockla A, et al. (2012) PRSS3/mesotrypsin is a therapeutic target for metastatic prostate cancer. *Mol Cancer Res* 10:1555–1566.
19. Aran D, et al. (2017) Comprehensive analysis of normal adjacent to tumor transcriptomes. *Nat Commun* 8:1077.
20. Withana NP, et al. (2016) Labeling of active proteases in fresh-frozen tissues by topical application of quenched activity-based probes. *Nat Protoc* 11:184–191.
21. Sobel RE, Sadar MD (2005) Cell lines used in prostate cancer research: A compendium of old and new lines–Part 1. *J Urol* 173:342–359.
22. Dudani JS, Buss CG, Akana RTK, Kwong GA, Bhatia SN (2016) Sustained-release synthetic biomarkers for monitoring thrombosis and inflammation using point-of-care compatible readouts. *Adv Funct Mater* 26:2919–2928.
23. Warren AD, Kwong GA, Wood DK, Lin KY, Bhatia SN (2014) Point-of-care diagnostics for noncommunicable diseases using synthetic urinary biomarkers and paper microfluidics. *Proc Natl Acad Sci USA* 111:3671–3676.
24. Gartrell BA, Saad F (2014) Managing bone metastases and reducing skeletal related events in prostate cancer. *Nat Rev Clin Oncol* 11:335–345.
25. Sugahara KN, et al. (2010) Coadministration of a tumor-penetrating peptide enhances the efficacy of cancer drugs. *Science* 328:1031–1035.
26. Sutherland M, Gordon A, Shnyder SD, Patterson LH, Sheldrake HM (2012) RGD-binding integrins in prostate cancer: Expression patterns and therapeutic prospects against bone metastasis. *Cancers (Basel)* 4:1106–1145.
27. Lundwall A, Clauss A, Olsson AY (2006) Evolution of kallikrein-related peptidases in mammals and identification of a genetic locus encoding potential regulatory inhibitors. *Biol Chem* 387:243–249.
28. Penna G, et al. (2007) Spontaneous and prostatic steroid binding protein peptide-induced autoimmune prostatitis in the nonobese diabetic mouse. *J Immunol* 179: 1559–1567.
29. Jiang M, Strand DW, Franco OE, Clark PE, Hayward SW (2011) PPARγ: A molecular link between systemic metabolic disease and benign prostate hyperplasia. *Differentiation* 82:220–236.
30. Böhm L, et al. (2013) uPA/PAI-1 ratios distinguish benign prostatic hyperplasia and prostate cancer. *J Cancer Res Clin Oncol* 139:1221–1228.
31. Morgia G, et al. (2005) Matrix metalloproteinases as diagnostic (MMP-13) and prognostic (MMP-2, MMP-9) markers of prostate cancer. *Urol Res* 33:44–50.
32. Ellwood-Yen K, et al. (2003) Myc-driven murine prostate cancer shares molecular features with human prostate tumors. *Cancer Cell* 4:223–238.
33. Pridgen EM, et al. (2013) Transepithelial transport of Fc-targeted nanoparticles by the neonatal Fc receptor for oral delivery. *Sci Transl Med* 5:213ra167.
34. Banerjee A, et al. (2018) Ionic liquids for oral insulin delivery. *Proc Natl Acad Sci USA* 115:7296–7301.